Mode Competition and Collision Effects in Gaseous Optical Masers

R. L. FORK AND M. A. POLLACK
Bell Telephone Laboratories, Murray Hill, New Jersey
(Received 26 March 1965)

This paper presents theoretical computer curves of the mode intensities and beat frequencies of a gaseous optical maser for oscillation on two axial modes, after the theory of Lamb. A modified form of Lamb's theory which includes collision effects is also given, and a comparison of experimental and theoretical curves as a function of pressure is made. The principal conclusions are that the modified theory shows good agreement with experiment and that the collision-induced asymmetry in the optical-field–atom interaction curve plays an important role in influencing optical-maser behavior.

INTRODUCTION

THIS paper describes a study of a gas optical maser under the condition of oscillation on two linearly polarized modes. The intent of the work is to provide an experimental check of the extensive optical-maser theory given by Lamb.[1] The value of an experimentally verified theory permitting reliable prediction of mode intensities, frequencies, and, under some conditions relative phases of the maser oscillations is obvious. Earlier workers have studied single-mode intensities[2,3] or have observed the beat frequency between two modes[4,5] as functions of resonator length and excitation. The major contribution of this work is the simultaneous observation of the beat frequency and mode intensities under the condition of two-mode operation, which permits a more sensitive and complete check of Lamb's theory than had been previously possible. In particular, the oscillator used restricted oscillation to a single linear polarization, a condition of Lamb's theory not satisfied by the earlier two-mode experiments.

Although qualitative agreement with Lamb's theory was found, particularly at low gas pressures, significant discrepancies were observed which we have attributed to atom-atom collisions. Of particular importance is the effect of collision-induced asymmetry in the stationary atom–optical-field interaction curve. Competition between modes for the available gain, principally near symmetrical disposition of the modes on the gain curve, is very sensitive to asymmetries in the interaction curve, providing a sensitive check of the collision-induced asymmetries. It was possible to introduce a modification of Lamb's theory which includes some of the principal effects of collisions and which produces substantial agreement between theory and experiment.

MODE AMPLITUDES AND FREQUENCIES COMPUTED FROM LAMB'S THEORY

By way of introducing the reader to the problem, we will briefly summarize Lamb's assumptions, examine the pertinent equations, and discuss the curves of mode intensity and beat frequency that result from a computer calculation using the theory. Lamb treats the maser as a high-Q multimode resonator in which there is a classical electromagnetic field interacting with a medium consisting of a collection of atoms in states a and b, described quantum-mechanically. He assumes that the field acts on the atoms to produce a macroscopic polarization and then solves the self-consistency equations given by applying Maxwell's equations to the system. He includes the effects of atomic motion (inhomogeneous Doppler broadening) but ignores the vector character (polarization) of the electromagnetic field. Uniform plane waves are assumed, and the calculation is carried out only to lowest order in the field intensity. The essential result of the calculation is equations determining the mode intensities and frequencies in terms of the unsaturated net gain α_n and dispersion σ_n, as well as certain saturation parameters β_n, θ_{nm}, ρ_n, τ_{nm} discussed below. We will be principally concerned with two-mode oscillation and hence will only reproduce the equations governing that regime.

Thus for oscillation on two adjacent axial modes, the amplitudes E_1 and E_2 are solutions of

$$\alpha_1=\beta_1E_1^2+\theta_{12}E_2^2 \tag{1a}$$

and

$$\alpha_2=\beta_2E_2^2+\theta_{21}E_1^2. \tag{1b}$$

The oscillation frequencies are given by

$$\nu_1=\Omega_1+\sigma_1+\rho_1E_1^2+\tau_{12}E_2^2 \tag{2a}$$

and

$$\nu_2=\Omega_2+\sigma_2+\rho_2E_2\sigma^2+\tau_{21}E_1^2. \tag{2b}$$

The resonant frequencies of the unperturbed cavity are given by Ω_n. The other coefficients are functions of the single-pass fractional loss l_0, the ratio of population inversion to threshold inversion η, the upper and lower state decay rates γ_a and γ_b, the Doppler width Ku, the location of the oscillation frequencies with respect to line center ω, the difference frequency $\Delta=(\Omega_2-\Omega_1)$, and a filling factor describing the distribution of the active medium in the resonator, N_2/N_0.

Some insight into Lamb's equations can be gained by relating the individual terms in Eqs. (1) and (2) to the physical processes in the maser. In the amplitude determining Eqs. (1), as mentioned above, α_n corre-

[1] W. E. Lamb, Jr., Phys. Rev. **134**, A1429 (1964).
[2] R. A. McFarlane, W. R. Bennett, Jr., and W. E. Lamb, Jr., Appl. Phys. Letters **2**, 189 (1963).
[3] A. Szöke and A. Javan, Phys. Rev. Letters **10**, 521 (1963).
[4] W. R. Bennett, Jr., Appl. Opt. Suppl. **1**, 24 (1962).
[5] R. A. McFarlane, Phys. Rev. **135**, A543 (1964).

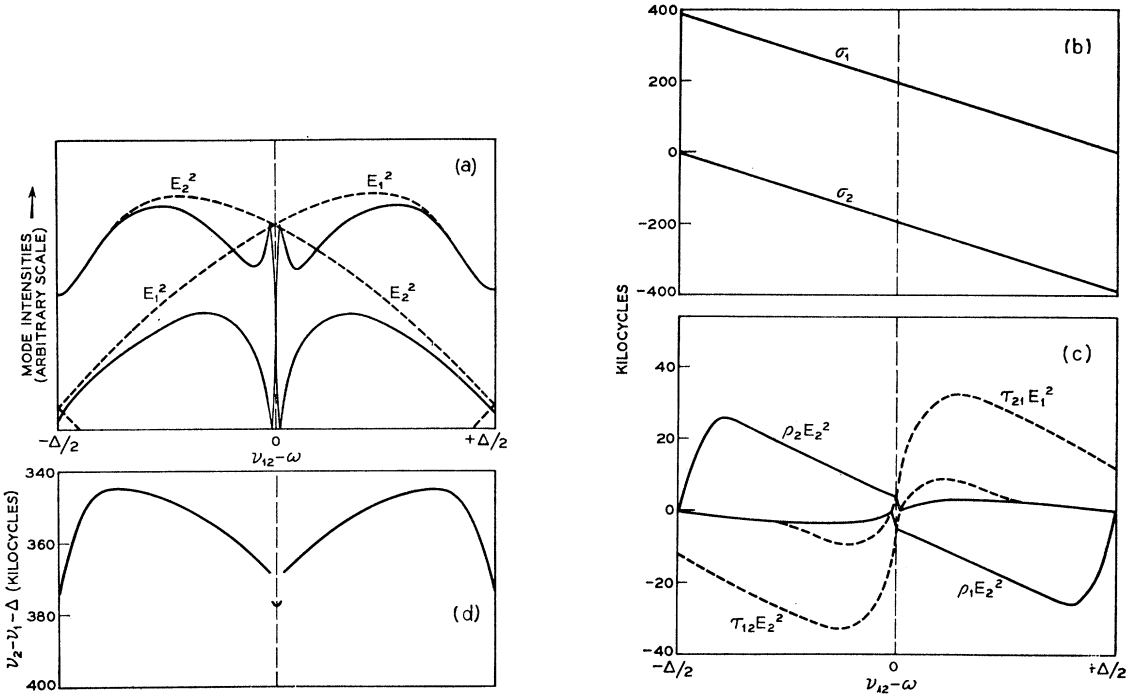

FIG. 1. (a) Theoretical curves showing typical mode intensities as a function of resonator tuning ($\nu_{12}-\omega$). The parameters for this example are: $\gamma_a=12$ Mc/sec, $\gamma_b=23$ Mc/sec, $Ku=1010$ Mc/sec, $\Delta=215$ Mc/sec, $l_0=0.044$, $\eta=1.05$, and $N_2/N_0=-0.56$. The dotted curves show the mode intensities for the case where the mode coupling is neglected ($\theta=0$). The solid curves show the mode intensities including the coupling terms. Vertical axis is given in arbitrary units for all the mode intensity curves. (b), (c) Theoretical curves showing typical dependence of the σ, ρ, and τ terms on resonator tuning. (d) Shows the corresponding beat-frequency curve as a function of resonator tuning.

sponds to the net single-pass unsaturated gain; $\beta_nE_n^2$ is the decrease in that net gain due to saturation (population depletion) of the gain curve by mode n, and $\theta_{nm}E_m^2$ is the decrease in the gain due to the saturation by mode m. In the frequency-determining Eqs. (2), the σ_n term represents the frequency shift of mode n caused by the dispersion of the unsaturated medium; $\rho_nE_n^2$ represents a decrease in the frequency shift of mode n which is caused by the saturation of the gain curve by mode n, and $\tau_{nm}E_m^2$ is a similar change caused by saturation of the gain curve by mode m.

Typical computer calculations[6] of the mode intensities as a function of the midfrequency $\nu_{12}=\frac{1}{2}(\nu_1+\nu_2)$ are shown in Fig. 1(a) (solid curve). The most striking feature is the rapid change in the ratio of intensities in the vicinity of midtuning. This rapid change is a consequence of the so-called "mode competition" which arises from the θ terms. By way of illustrating the effects of mode competition, we have included a computer calculation of the expected mode intensities with the θ coefficients set equal to zero, i.e., in the absence of mode competition (dashed curve). Such a condition might be approximated in a traveling-wave ring maser, for example, where the mode coupling can be small. The effect of the mode competition can be regarded as the reduction of gain available to one mode caused by saturation by another mode. In the two-mode case, the gain available to mode 1 is $\alpha_1-\theta_{12}E_2^2$. If $\theta_{12}E_2^2\geq\alpha_1$, then mode 1 cannot oscillate, and for the region of tuning over which this condition exists only one mode oscillation is observed. Such behavior was typical of the experimental results.

The individual frequency terms of Eqs. (2a) and (2b) are plotted for the same example in Fig. 1(b) and (c). The sign of a given $\rho_nE_n^2$ term remains the same over the entire tuning curve, the sign depending on whether $\nu_n\gtrless\omega$. The effect of the $\rho_nE_n^2$ term is always to shift the frequency of oscillation away from line center.

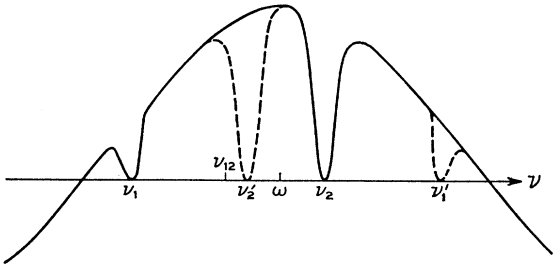

FIG. 2. Population depletion holes in the velocity distribution for two oscillation frequencies, shown on a frequency scale. Holes produced by the field component traveling to the right are shown by solid curves. Holes produced by the field component traveling to the left are shown by dotted curves.

[6] Although only the equations for two-mode operation have been given, all the theoretical curves have been computed taking into account three possible oscillating modes for $\nu_{12}\approx\pm\Delta/2$. Decay rates for the sample computer calculation were obtained from the lifetimes given in Ref. 16 for the Ne $3s_2$-$2p_4$ maser.

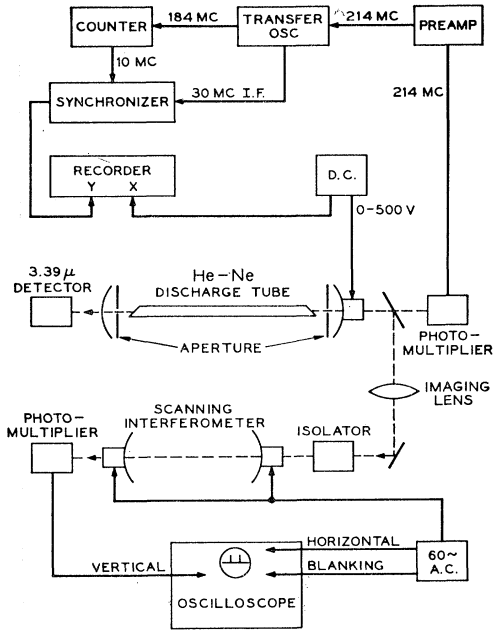

FIG. 3. Block diagram of the experimental apparatus.

The $\tau_{nm}E_m^2$ terms are more complex in that each of the $\tau_{nm}E_m^2$ terms can be either negative or positive depending on the position of the modes on the gain curve. That is, the saturation due to the τ_{nm} terms can shift the frequency of oscillation either away from or toward line center. However, since $(\tau_{21}E_1^2-\tau_{12}E_2^2)$ is always positive, the net effect of the τ terms on the beat frequency $(\nu_2-\nu_1)$ is to increase it. The same conclusions can be reached by applying the rule that the population holes[7] shown in Fig. 2 repel each other.[8] The beat frequency $\nu_2-\nu_1$ is shown in Fig. 1(d). The most obvious feature is the dip in the curve at midtuning.

It should be noted that the mode intensities and the beat frequency are symmetric functions of tuning. This is a necessary consequence of the symmetry of the interaction curve used. Mode competition alone does not introduce asymmetries into the intensity or beat-frequency patterns.

EXPERIMENTAL APPARATUS

To verify the details of Lamb's theory, a He^3-Ne^{20} maser was operated on the 0.633-μ ($3s_2$-$2p_4$) Ne^{20} transition, and the mode amplitudes and beat frequency measured as functions of the resonator length. The maser oscillator consisted of a Brewster window, 3-mm i.d. dc discharge tube, with external two-meter-radius dielectric coated mirrors of nearly equal reflectivity. One mirror was mounted on a piezoelectric transducer, permitting the resonator modes to be scanned across the Doppler line as the resonator length was changed slowly by several half wavelengths. The discharge length of 40 cm was nearly centered in the 70-cm-long resonator. The resonator length was stabilized by means of quartz spacing bars between the mirror mounts. All the optical components were fastened to an air-supported mounting to reduce vibrations. The space between windows and mirrors was enclosed to reduce airborne disturbances. This space was filled with methane at atmospheric pressure to absorb the competing 3.39-μ ($3s_2 \rightarrow 3p_4$) radiation, since oscillation on that transition was noted to be a spurious source of mode suppression. Apertures were inserted in the resonator to eliminate off-axis modes, and to restrict operation to two axial modes. Enriched Ne^{20} (99.99%) isotope was employed in the discharge to remove the large gain curve asymmetry of naturally occurring mixed isotope neon. To permit variation of Ne^{20} and He^3 pressures, the tube was permanently connected to a gas-handling station.

The system used to measure mode intensities and beat frequencies is shown in Fig. 3. Part of the maser output was directed to a lead selenide detector, to check on the absence of 3.39 μ oscillation. Output from the opposite end of the maser was split, with a small fraction falling on the cathode of a photomultiplier. The ~214-Mc/sec beat signal was amplified and fed to an oscillator-synchronizer system identical to the one used by McFarlane[5] for similar beat-frequency measure-

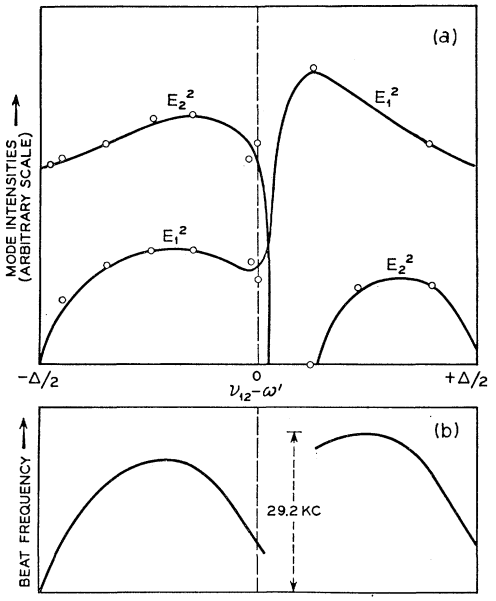

FIG. 4. Experimental curves of two-mode intensities and beat frequency versus resonator tuning. The Ne^{20} pressure was 0.15 Torr and the He^3 pressure 0.42 Torr. The circles correspond to measurements of photographs taken of the oscilloscope display for particular resonator lengths. The solid line represents a connection of the points arrived at on the basis of usual observation of the oscilloscope display during tuning of the resonator.

[7] The term "hole" was introduced by Bennett to describe the population depletions in certain frequency ranges of the gain curve caused by saturation, and we use the term in the same sense. The "holes" described by the saturations terms will be somewhat different from those given by Bennett in that they arise from a more rigorous analysis.

[8] This rule is a simple consequence of the fact that the correction to the dispersion of the gain curve required by a hole is a dispersion curve of opposite sign to that of the gain curve.

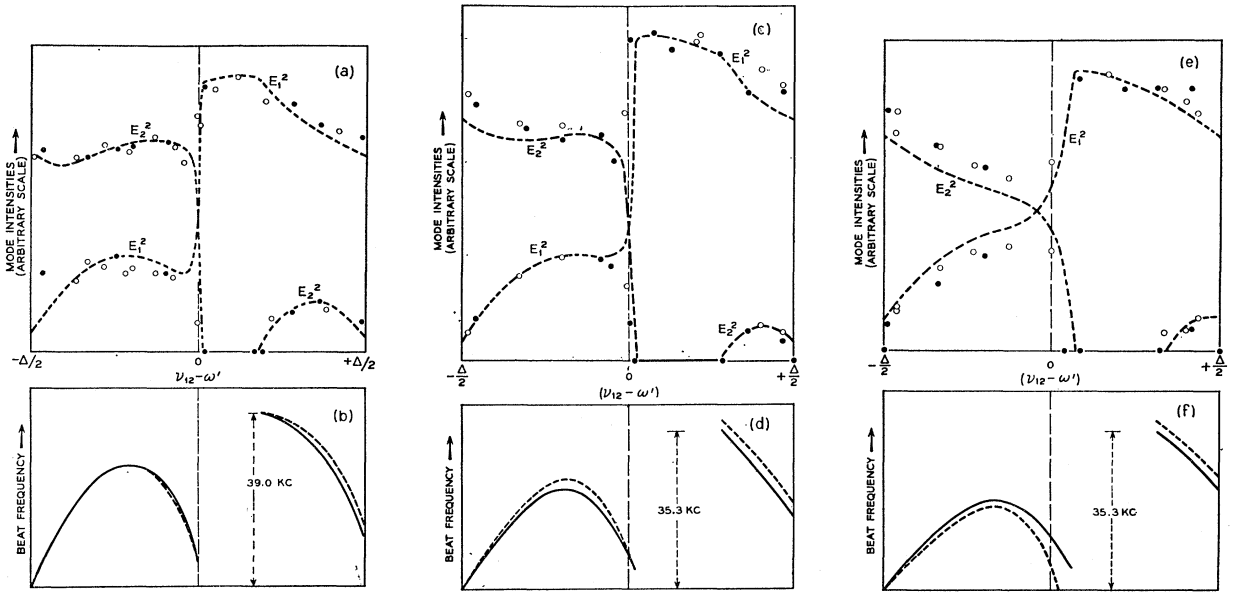

FIG. 5. Experimental and theoretical curves of mode intensities and beat frequencies versus resonator tuning for three different pressures of He^3: 0.6 (a), (b), 1.0 (c), (d), and 1.4 (e), (f) Torr. The Ne^{20} pressure was 0.15 Torr, in each case. The experimental mode intensities are indicated by two sets of points taken in successive runs and the experimental beat frequency is indicated by a solid line. The theoretical curves are shown as dashed lines in intensity and frequency plots.

ments. The beat frequency was displayed directly on an x-y recorder, while a counter was used for system calibration.

The remainder of the split maser output was passed through a scanning spherical-mirror interferometer[9] to a second photomultiplier. An oscilloscope, swept and blanked in synchronism with the sinusoidal interferometer sweep, displayed the photomultiplier output and allowed direct measurement of the mode intensities. At least 30 dB of isolation was used between the scanning interferometer and the maser resonator to prevent spurious coupling.

EXPERIMENTAL RESULTS

The loss at the internal apertures was adjusted to permit two-frequency oscillation with a discharge current of about 10 mA. Figure 4 shows experimental curves of the intensities of the oscillations at frequencies ν_1 and ν_2 and the beat frequency $\nu_2-\nu_1$ as functions of $(\nu_{12}-\omega')$. The frequency ω' is midway between the frequencies at which one mode drops below oscillation threshold and another mode begins oscillation ($\omega'\sim\omega$.) The curves shown were observed at gas pressures of 0.15 Torr Ne^{20} and 0.42 Torr He^3, close to the lowest pressures at which oscillation could be obtained. This case corresponds most closely to Lamb's theory, in that the collision broadening is minimized.

The basic features of the experimental curves agree with the competition and frequency variation predicted by Lamb's theory (see Fig. 1). Figure 4, however, shows a wider region of intensity crossover and a marked asymmetry with the high-frequency oscillation completely quenched for ν_{12} greater than ω', whereas the low-frequency oscillation is only slightly depressed for ν_{12} less than ω'. The maximum frequency variation is greater above ω' than below. In addition, there is a discontinuous jump in beat frequency at the point at which one mode starts to drop below oscillation threshold, one mode is near line center, and a new mode

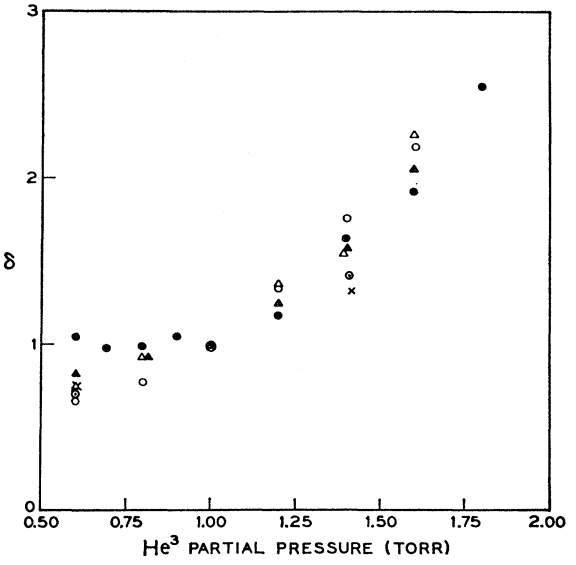

FIG. 6. Variation of the beat-frequency jump δ with He^3 partial pressure. Values of δ from several runs at slightly different excitation levels are shown normalized to the value of δ at 1.0 Torr He^3. Partial pressure of Ne^{20} is 0.15 Torr. The crosses indicate values obtained from the fit with theory.

[9] R. L. Fork, D. R. Herriott, and H. Kogelnik, Appl. Opt. 3, 1471 (1964).

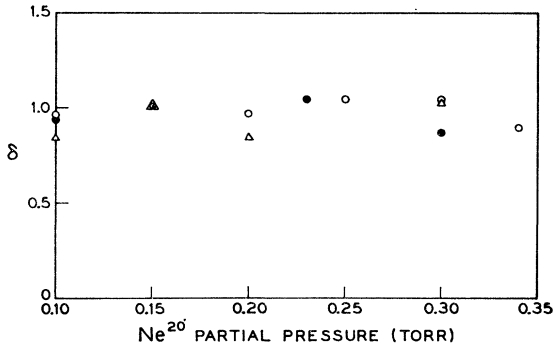

FIG. 7. Variation of the beat-frequency jump δ with Ne^{20} partial pressure. Values of δ from several runs are shown normalized to the value of δ at 0.15 Torr Ne^{20}. Partial pressure of He^3 is 1.0 Torr.

begins oscillation ($\nu_{12}-\omega'=\pm\Delta/2$). This frequency jump δ can be used as a measure of the asymmetry in the beat-frequency curve. One might expect three- rather than two-mode oscillation at $(\nu_{12}-\omega')=\pm\Delta/2$; however, because of competition between the two modes at $\nu=\omega\pm\Delta$ near their oscillation threshold, the excitation level must be increased well above this threshold before three-frequency oscillation is reached.

To examine the pressure dependence of the asymmetry, a range of He^3 pressures was covered. Figure 5 shows the mode intensities and beat frequencies for typical He^3 pressures of 0.6, 1.0, and 1.4 Torr with 0.15 Torr Ne^{20}. This set was taken with a constant cavity loss, which was different from that used to obtain Fig. 4. Note that the width of the "quenched" region, the beat-frequency jump, and the general asymmetry all increase with He^3 pressure. Figure 6 shows the variation of δ with He^3 partial pressure at a Ne^{20} partial pressure of 0.15 Torr, normalized to δ at 1.0 Torr He^3. The points are average values of δ taken from several different runs. The dependence of the frequency jump on He^3 pressure is obvious. Fig. 7, which shows the variation of δ with Ne^{20} pressure at a He^3 partial pressure of 1.0 Torr normalized to δ at 0.15 Torr Ne^{20}, indicates that there is no strong Ne^{20} pressure dependence of the frequency jump.

Several checks were made to assure that the observed asymmetries did not result from spurious effects. The asymmetrical intensity and beat frequency curves were obtained with either rf or dc excitation of the discharge, and were highly reproducible, independent of resonator alignment. As noted above, factors that could cause asymmetrical frequency dependence of the gain or loss, such as oscillation at 3.39 μ, or substantial amounts of Ne^{22} isotope, were eliminated. A calculation using Lamb's theory showed that the upper limit on the experimental isotope ratio Ne^{22}:Ne^{20} of 1:10 000 would introduce a negligible asymmetry which was of the opposite sign of that observed.

Some difficulty was initially encountered with spurious mode suppression arising from the frequency dependence of the effective mirror reflectivities. Reflections from the second surface of the mirror back into the mode volume of the resonator can cause periodic variations of the mirror reflectivity due to interference.[10] By keeping the intersurface mirror resonances far from the Doppler line center, however, this effect of mode suppression was made negligible in the experiment. A control experiment was run with wedged mirrors, with which no light could be reflected from the second surface back into the resonator mode volume and identical asymmetrical intensity and beat-frequency patterns were observed.

In addition, the beat-frequency variation was examined qualitatively for a maser oscillating on the 1.15-μ ($2s_2$-$2p_4$) Ne^{20} transition, and a similar asymmetrical pattern was obtained.

MODIFICATIONS OF THEORY TO INCLUDE COLLISIONS

Since it was not possible to fit the experimental data quantitatively with curves of the form shown in Fig. 1, some modification of Lamb's theory was required. As Szöke and Javan[3] have already noted, the so-called soft-collision[11] process produces changes in the atom–optical-field interaction which cannot be described by simply increasing the decay rates γ_a and γ_b for the states involved. Both a change in the phase of oscillation and a velocity shift occur in the collision process; however, Szöke and Javan were able to fit their data for the single-mode central tuning dip by considering only the velocity shift. We have chosen to consider the effect of the change in the phase of oscillation and to neglect the velocity shift. A consideration of both effects is rather complicated,[12] and the essential features of our experiment can be matched with our simpler model. It should be noted that the velocity-shift model is inadequate to explain our results, principally because the velocity shift introduces no asymmetries. Even small asymmetries in atomic response apparently need to be included in the two-mode problem because the mode competition, seen in the θ terms, is particularly sensitive to asymmetries. The central tuning dip, seen in the β term, is less sensitive to asymmetries but may still show their effects.[13]

The maser levels will be perturbed by nonresonant collisions with He^3 atoms and by resonant and non-

[10] H. Kogelnik and C. K. N. Patel, Proc. IRE **50**, 2365 (1962).

[11] We follow the convention that defines a hard collision as one in which the phase shift of the colliding atom is greater than 2π and a soft collision as one in which the phase shift is less than 2π. That is, in a hard collision the atom is effectively removed from the interaction, the process being describable simply by a change in the decay rate for the state, whereas in the soft collision the interaction continues, but the phase shift appears as a change in the atomic response curve, the essential changes being a broadening, a frequency shift of the line center, and the introduction of an asymmetry.

[12] W. Lamb and B. Gyorffy are making such a calculation (private communication).

[13] Dr. Javan recently observed a pressure-dependent asymmetry in single-mode intensity curves (private communication).

resonant collisions with Ne^{20} atoms. The additional complication of treating the resonant collisions separately has been neglected. For our atomic response curve, we have taken the curve given by Anderson and Talman[14] derived from a consideration of the Van der Waal's forces of nonresonant collisions,

$$D(\nu-\omega_S)=e^{ic}/[\gamma_{ab}'-i(\nu-\omega_S)]. \quad (3)$$

In the Anderson-Talman theory, c, γ_{ab}, and $\omega_S-\omega$ are linear functions of pressure. Substitution of (3) for the atomic response mixes the real and imaginary parts of the coefficients of (1) and (2) as given by Lamb. The appendix gives the coefficients, modified by the insertion of (3) into Lamb's theory. These coefficients have an additional difference from Lamb's in that terms of the order γ_{ab}/Δ have not been neglected. The dashed intensity and beat-frequency curves[15] shown along with the experimental curves in Fig. 5 were computed using the modified coefficients of the appendix. Figure 8 gives the parameters adjusted to fit the experimental curves at the three pressures examined. The computed curves are insensitive to changes in γ_a and γ_b and depend primarily on γ_{ab}', c, and η. A previous experiment[16] was used to determine γ_a and γ_b at 0.7 Torr He, while γ_b at the zero-pressure limit was taken from Bennett[4] to be 13 Mc/sec and γ_a at zero pressure was estimated to be 10 Mc/sec.

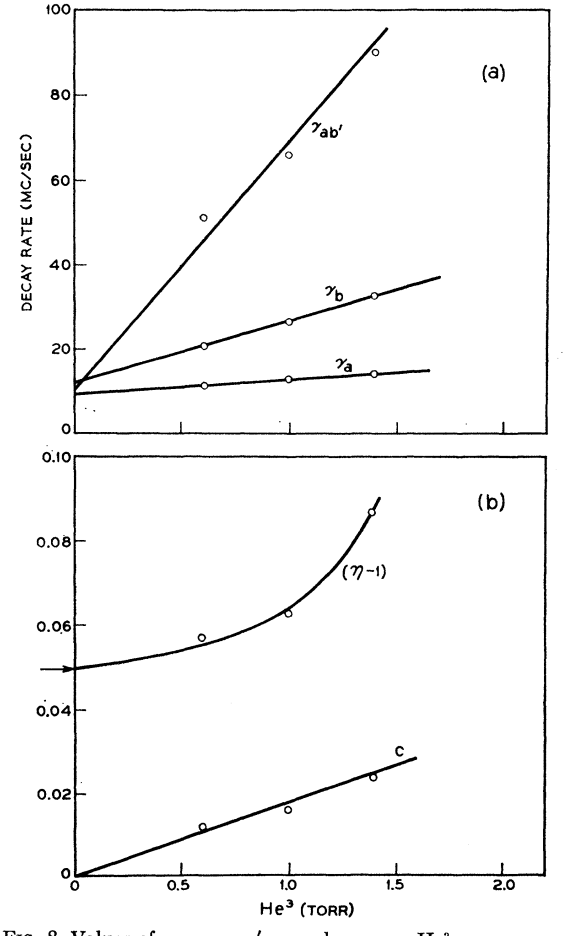

FIG. 8. Values of γ_a, γ_b, γ_{ab}', c, and η versus He^3 pressure used to fit the modified theory to the data (circled points). The arrow indicates the value of η required for three-mode threshold, neglecting competition effects and assuming only Doppler broadening. Fixed parameters are $Ku=1010$ Mc/sec (corresponding to 500°K), $l_0=0.044$, $\Delta=215$ Mc/sec, and $N_2/N_0=-0.56$.

We have noted that the slope of the linewidth-versus-pressure curve evaluated here for the $3s_2$-$2p_4$ transition is greater than that observed by Szöke and Javan in their study of the $2s_2$-$2p_4$ transition. The sign of the asymmetry as seen in the beat-frequency curves is the same for both transitions; however, the asymmetry appears to be greater for the $3s_2$-$2p_4$ transitions than for the $2s_2$-$2p_4$ transition. In addition, we note that the asymmetry favors the low-frequency mode, implying a shift to the red. These observations are consistent with the expected energy shift of the levels given by applying the energy-shift formula of Margenau and Watson.[17]

CONCLUSIONS

The essential conclusion of the work is that while Lamb's theory describes the general features of the mode intensity and beat-frequency curves as a function of resonator tuning, the effect of collision processes must be included to obtain detailed agreement of theory and experiment for typical operating pressures. In particular, the asymmetry of the interaction strength versus frequency must be included.

It would appear from the agreement of theory and experiment that the neglect of velocity broadening is not too serious. The difficulty of experimentally separating the velocity broadening from the Van der Waal's broadening at present lessens the importance of making a theoretical distinction. Since the velocity broadening should be more important near line center, we suggest that a comparison of the one-mode and two-mode data, which are most sensitive to the broadening at line center and removed from line center by a half-mode spacing, respectively, might assist in separating the two effects. We noted that an attempt to fit one-mode data with our theory required a larger broadening and smaller asymmetry for a given pressure than was required by the two-mode data, suggesting that the broadening increases toward line center, and more of the broadening is produced by a symmetric process such as the velocity shift.

[14] P. W. Anderson and J. D. Talman, Proceedings of the Conference on Broadening Spectral Lines, p. 29, 1956 (unpublished).

[15] Since the passive cavity-mode spacing Δ could not be measured accurately, only the beat-frequency variation has been given, and not the total frequency. The theoretical and experimental curves were aligned at the beat-frequency minimum. The factor l_0 was chosen to fit the theoretical spread of beat frequency to the experimental spread in Fig. 5(b) and was consistent with the expected value.

[16] R. L. Fork, L. E. Hargrove, and M. A. Pollack, Appl. Phys. Letters 5, 5 (1964).

[17] H. Margenau and W. W. Watson, Rev. Mod. Phys. 8, 22 (1936).

ACKNOWLEDGMENTS

The authors have profited from many discussions with Professor W. E. Lamb, Jr., and would like to specifically thank M. Lax and P. W. Anderson for their comments on the collision line shape. The assistance of L. Heilos and W. R. Wolff in the fabrication of equipment and the operation of the experiment is greatly appreciated.

APPENDIX: COLLISION MODIFICATION TO COEFFICIENTS

$$\alpha_n=\alpha_n'\cos c+\sigma_n'\sin c-(l_0\Delta/2\pi)(1-\cos c),$$
$$\sigma_n=\sigma_n'\cos c-[\alpha_n'+(l_0\Delta/2\pi)]\sin c,$$
$$\beta_n=\beta_n'\cos c-\rho_n'\sin c,$$
$$\rho_n=\rho_n'\cos c+\beta_n'\sin c,$$
$$\theta_{nm}=\theta_{nm}'\cos c-\tau_{nm}'\sin c,$$
$$\tau_{nm}=\tau_{nm}'\cos c+\theta_{nm}'\sin c,$$

where

$$\alpha_n'=\eta\frac{l_0\Delta}{2\pi}\left[\frac{Z_i(\nu_n-\omega)}{Z_{\max}}-\frac{1}{\eta}\right],$$
$$\sigma_n'=\eta\frac{l_0\Delta}{2\pi}\left[\frac{Z_r(\nu_n-\omega)}{Z_{\max}}\right],$$
$$\beta_n'=F[1+\gamma_{ab}'^2\mathfrak{L}(\nu_n-\omega)],$$
$$\rho_n'=F\gamma_{ab}'(\nu_n-\omega)\mathfrak{L}(\nu_n-\omega),$$
$$\theta_{nm}'=F\Big\{\gamma_{ab}'^2\Big[\mathfrak{L}(\omega-\nu_{12})+\mathfrak{L}\Big(\frac{\Delta}{2}\Big)\Big]+\frac{\gamma_a\gamma_b}{2}\frac{\gamma_{ab}'}{\gamma_{ab}}\Big[\gamma_{ab}'\Big(\frac{\gamma_a}{\gamma_a^2+\Delta^2}+\frac{\gamma_b}{\gamma_b^2+\Delta^2}\Big)-\frac{\Delta}{2}\Big(\frac{\Delta}{\gamma_a^2+\Delta^2}+\frac{\Delta}{\gamma_b^2+\Delta^2}\Big)\Big]\mathfrak{L}\Big(\frac{\Delta}{2}\Big)+\frac{N_2}{N_0}\frac{\gamma_a\gamma_b}{2}\frac{\gamma_{ab}'}{\gamma_{ab}}\Big[\gamma_{ab}'\Big(\frac{\gamma_a}{\gamma_a^2+\Delta^2}+\frac{\gamma_b}{\gamma_b^2+\Delta^2}\Big)\mp(\omega-\nu_n)\Big(\frac{\Delta}{\gamma_a^2+\Delta^2}+\frac{\Delta}{\gamma_b^2+\Delta^2}\Big)\Big]\mathfrak{L}(\omega-\nu_n)\Big\},$$

$$\tau_{nm}'=-F\Big\{\gamma_{ab}'(\omega-\nu_{12})\mathfrak{L}(\omega-\nu_{12})\pm\gamma_{ab}'\frac{\Delta}{2}\mathfrak{L}\Big(\frac{\Delta}{2}\Big)\pm\frac{\gamma_a\gamma_b}{2}\frac{\gamma_{ab}'}{\gamma_{ab}}\Big[\frac{\Delta}{2}\Big(\frac{\gamma_a}{\gamma_a^2+\Delta^2}+\frac{\gamma_b}{\gamma_b^2+\Delta^2}\Big)+\gamma_{ab}'\Big(\frac{\Delta}{\gamma_a^2+\Delta^2}+\frac{\Delta}{\gamma_b^2+\Delta^2}\Big)\Big]\mathfrak{L}\Big(\frac{\Delta}{2}\Big)+\frac{N_2}{N_0}\frac{\gamma_a\gamma_b}{2}\frac{\gamma_{ab}'}{\gamma_{ab}}\Big[(\omega-\nu_n)\Big(\frac{\gamma_a}{\gamma_a^2+\Delta^2}+\frac{\gamma_b}{\gamma_b^2+\Delta^2}\Big)\pm\gamma_{ab}'\Big(\frac{\Delta}{\gamma_a^2+\Delta^2}+\frac{\Delta}{\gamma_b^2+\Delta^2}\Big)\Big]\mathfrak{L}(\omega-\nu_n)\Big\},$$

where the upper sign holds for $m=n+1$ and the lower sign holds for $m=n-1$;

$$\gamma_{ab}=(\gamma_a+\gamma_b)/2,\quad \gamma_{ab}'=\gamma_{ab}+\text{constant}\times\text{pressure},$$
$$\mathfrak{L}(x)=1/(\gamma_{ab}'^2+x^2),$$
$$N_n=\frac{1}{L}\int_0^L dz N(z)\cos\Big(\frac{n\pi z}{L}\Big),$$

$[N(z)=\text{inversion density}]$,

$$Z(\nu-\omega)=Z\Big(\frac{\nu-\omega}{Ku}+i\frac{\gamma_{ab}'}{Ku}\Big)=Z(\zeta)$$
$$=2i\int_{-\infty}^{i\zeta}dt\exp-(t^2+\zeta^2),$$

$Z_{\max}=$ maximum value of $[Z_i(\nu-\omega)\cos c+Zr(\nu-\omega)\sin c]$,

and

$$F=\frac{\eta l_0\Delta}{Z_{\max}\gamma_a\gamma_b}\frac{\gamma_{ab}}{\gamma_{ab}'}\Big[\frac{\mathcal{P}^2}{16\pi^{\frac{1}{2}}\hbar^2}\Big],$$

where $\mathcal{P}$ is the electric-dipole matrix element.